Available online at www.sciencedirect.com
ScienceDirect
Journal of Molecular Catalysis A: Chemical 270 (2007) 164–170
JOURNAL OF MOLECULAR CATALYSIS A: CHEMICAL
www.elsevier.com/locate/molcata

A theoretical investigation of the adsorption surface sites of the activated $MgCl_2$

Dmitry A. Trubitsyn *, Vladimir A. Zakharov, Ivan I. Zakharov

Boreskov Institute of Catalysis, 630090 Novosibirsk, Russia

Received 25 January 2006; received in revised form 29 December 2006; accepted 29 December 2006
Available online 16 January 2007

Abstract

The adsorption of carbon monoxide on activated $MgCl_2$ has been investigated within DFT using different models of the $MgCl_2$ surface. All the models were Mg_6Cl_{10} clusters with two saturating OH groups. It has been found that the adsorption sites within the models based on the geometry of the ideal $MgCl_2$ crystal are stronger than they are in the experiment. It has also been found that relaxed clusters based on the geometry of the relaxed $MgCl_2$ surface present more accurate models of the $MgCl_2$ surface and account the relaxation effects properly. IR spectra of carbon monoxide bounded to three different adsorption sites calculated within relaxed clusters approximation is in excellent agreement with the experimental data. Such an agreement allows us to conclude that adsorption sites of the activated $MgCl_2$ surface in general are 3-, 4- and 5-fold Mg atoms and the structure of these sites follows the structure of corresponded relaxed $MgCl_2$ crystallographic faces.

Keywords: IR spectra; Quantum chemistry; Magnesium chloride; Carbon monoxide; Ziegler–Natta catalysts

1. Introduction

Identification of the active catalytic sites is one of the most important challenges in a $MgCl_2$-supported Ziegler–Natta polymerization catalysis system used for polyolefin production [1,2]. The ability to distinguish active sites on the Ziegler–Natta catalysts can provide an unprecedented opportunity to correlate catalytic behaviors, such as polymerization activity and stereospecificity, with surface structure and composition. In turn, molecular-level knowledge of the adsorption sites structure on the $MgCl_2$ surface is a prerequisite to controlling the active sites of the heterogeneous catalyst.

A number of papers is devoted to the experimental [3–7 and references therein] and theoretical [8–11 and references therein] determination of the structure of the active sites in Ziegler–Natta catalysts. Among them many experimental studies were carried out using Infra Red (IR) spectroscopy techniques.

In ref. [7] diffuse reflectance IR spectroscopy has been used to study carbon monoxide adsorption on highly dispersed magnesium chloride. The authors observed IR bands at 2210, 2190 and 2170 cm^{-1} upon adsorption of carbon monoxide on the various samples of magnesium chloride. These three bands were attributed to carbon monoxide chemisorbed on three different cations (low-coordinate magnesium ions) of the magnesium chloride lattice.

In ref. [11] the authors applied semiempirical quantum-chemical methods to describe the adsorption centers of magnesium chloride and to simulate chemisorption of carbon monoxide on its surface. As the result, experimental bands 2210, 2190 and 2170 cm^{-1} were attributed to the adsorption complexes of carbon monoxide with 3-, 4- and 5-coordinate magnesium atoms of magnesium chloride, respectively. However, all the obtained results were barely qualitative. The calculated IR spectra of adsorbed carbon monoxide differed significantly from the experimental spectra.

In this paper we determine the approach within density functional theory (DFT), which provides agreement better than 10 cm^{-1} between calculated and experimental IR spectra of carbon monoxide bounded to the $MgCl_2$ surface. Such an agreement allows us to find out the molecular structure of the $MgCl_2$ surface adsorption centers.

We simulate the adsorption of carbon monoxide on the $MgCl_2$ surface and calculate corresponding IR spectra within DFT using different models of the surface. All the models are relatively

* Corresponding author. Tel.: +7 383 330 60 64.
E-mail address: tda@catalysis.ru (D.A. Trubitsyn).

1381-1169/$ – see front matter © 2007 Elsevier B.V. All rights reserved.
doi:10.1016/j.molcata.2006.12.046

small magnesium chloride clusters with the same stoichiometry Mg_6Cl_{10}. However, surface relaxation effects are accounted in these clusters differently.

In the first model relaxation effects are not considered at all. The clusters are based on the geometry of the ideal $MgCl_2$ crystal (so-called, ideal clusters) with the well known structure. Magnesium and chlorine atoms inside these ideal clusters are always fixed. In the second model relaxation effects are simulated by the unfreezing of the adsorption site. The third model is entirely based on the geometry of the relaxed $MgCl_2$ surface. To build this model we optimize the geometry of free $MgCl_2$ crystallographic faces using a plane-wave pseudopotential approach within DFT and then cut Mg_6Cl_{10} clusters out from obtained relaxed surfaces and freeze them up.

2. Computational details

Geometry of the bulk $MgCl_2$ was calculated using periodic (infinite) $MgCl_2$ model. Calculations were performed using a plane-wave pseudopotential approach within DFT. Three different approximations were used for the exchange-correlation functional: one local, i.e. the local density approximation (LDA) [12], and two gradient corrected, i.e. the Perdew–Burke–Ernzerhof (PBE) [13] and Perdew–Wang (PW91) [14] functionals.

For each exchange-correlation functional a consistent norm-conserving [15] or ultrasoft [16] pseudopotential was used for both magnesium and chloride. Valence states include 3s states for Mg (2 electrons) and 3s and 3p states for Cl (7 electrons). The smooth part of wavefunctions is expanded in plane waves, with a kinetic energy cutoff of 25 Ry, while the cutoff for the augmented electron density is 200 Ry. For the bulk calculations 4 mesh × 4 mesh × 4 mesh of k points was used to sample the Brillouin zone.

Surface calculations were performed using LDA exchange-correlation functional, since test calculations indicate that this functional is the most accurate for $MgCl_2$ local geometry determination (see Section 3). For the surface calculations we used 8 mesh × 8 mesh × 1 mesh of k points in the Brillouin zone. The periodically repeated slabs were separated one from another by a vacuum region ∼10 Å wide. The experimental lattice constants were used. All the "periodic" calculations were performed using PWSCF [17] package.

The adsorption of carbon monoxide was simulated using cluster (finite) $MgCl_2$ model. Three different types of clusters were used: ideal cluster cutout from the bulk of $MgCl_2$ with totally frozen geometry, the same cluster with the unfrozen adsorption site and frozen relaxed clusters cutout from the calculated relaxed $MgCl_2$ surfaces. All clusters were Mg_6Cl_{10} with two saturating OH groups. While the geometry of the clusters was fixed in the calculations here reported (except adsorption site in some cases), the geometries of carbon monoxide and two OH groups were fully optimized.

All the "cluster" calculations were carried out within DFT with hybrid three-parameter Becke's exchange-correlation functional B3LYP [18]. The standard all-electron basis 6-31G(d) was employed for atoms H, C, O, Mg and Cl. The calculated harmonic frequencies in IR spectra were scaled by factor sf = 0.970. This factor is equal to the ratio between experimental and calculated frequency of the gaseous ν(C=O) vibration. All the "cluster" calculations were performed using Gaussian 98 package [19].

3. The structure of the bulk $MgCl_2$

As a prerequisite for the subsequent calculations it is necessary to briefly examine how well the computational methods perform for magnesium chloride.

$MgCl_2$ exists as a two crystalline forms: the first one is α-$MgCl_2$ ($R3m$ or $P1$) with the chloride anions organized in a face-centered cubic arrangement and the Mg cations in the octahedral interstices; the primitive cell is rhombohedric and the conventional cell hexagonal. It is more stable than β-$MgCl_2$ (Cm) with the chloride anions organized in a hcp arrangement [20].

The two forms differ only by the stacking of hexagonal layers: ABC BCA CAB ... or ABC ABC ABC ... for the α-$MgCl_2$ and β-$MgCl_2$, respectively. The internal structures of hexagonal layers in both cases are almost equivalent since van der Waals interaction between layers is weak.

To determine the lattice constants ($a = b$, c) of β-$MgCl_2$, the crystal internal geometry was fully optimized on a grid of points in the two-dimensional parameter ($a = b$, c) space. The minimum-energy configurations were obtained by interpolation and are compared to experimental data [20] in Table 1.

Let us note that the lattice constant c determines the distance between weakly interacting (attracting) $MgCl_2$ layers, thus the total energy of the system depends on this constant weakly. Speaking more precisely, total energy as a function of c has a very wide minimum that results in low precision of the lattice constant c determination (see Table 1).

It can be seen from Table 1 that the PW91 exchange-correlation functional in combination with the consistent ultrasoft pseudopotential (PW91/USP) provides the best accu-

Table 1
Lattice constants ($a = b$, c) and internal crystal geometry of β-$MgCl_2$: values obtained with different DFT approaches are compared with the experimental values

	Cell		Internal parameters		
	$a = b$ (Å)	c (Å)	Cl–Mg–Cl (°)	Mg–Cl–Mg (°)	Mg–Cl (Å)
Expt.	3.641	5.927	86.06	93.94	2.4873
LDA/NCP	3.55 (−2.5%)	∼6	86.1	93.9	2.49
PBE/NCP	3.73 (+2.5%)	∼6	87.6	92.4	2.52
PW91/USP	3.69 (+1.3%)	∼6	87.2	92.8	2.51

racy of the lattice constants determination. Whereas the LDA exchange-correlation functional in combination with the norm-conserving pseudopotential (LDA/NCP) provides the most accurate determination of the local $MgCl_2$ geometry, i.e. distances Mg–Cl and angles Cl–Mg–Cl and Mg–Cl–Mg.

4. The structure of the main $MgCl_2$ surfaces

In this section we analyze the atomic relaxations on the $MgCl_2$ surfaces. First of all let us comment on which $MgCl_2$ crystallographic faces are under consideration.

The basal (0 0 1) plane is energetically the most favorable, but it contains chlorine atoms only and, consequently, does not take part in the adsorption of any Lewis bases and as the result is out of the scope of active catalytic sites formation. Hence, (0 0 1) plane is out of our interest. The surface of non-activated $MgCl_2$ powder is presented mainly by this inactive (0 0 1) plane.

Activation processes (mechanical or chemical) of the $MgCl_2$ increase the portion of (1 1 0) and (1 0 0) crystallographic faces on the $MgCl_2$ surface [21,22]. These (1 1 0) and (1 0 0) surfaces contain 4- and 5-fold Mg atoms, respectively (Figs. 2 and 3) and are suitable for Lewis bases adsorption. For the sake of simplicity we will refer to these surfaces as to (1 1 0) (4-fold) and (1 0 0) (5-fold), respectively.

As it was already mentioned, the authors in [7,11] found that there are mainly three types of the adsorption sites on the activated $MgCl_2$ surface. These sites are 3-, 4- and 5-fold Mg atoms.

In concordance with these facts we suppose that 4- and 5-fold adsorption sites are basically presented by (1 1 0) (4-fold) and (1 0 0) (5-fold) $MgCl_2$ crystallographic faces, respectively. Hence, the calculated geometry of the relaxed (1 1 0) (4-fold) and (1 0 0) (5-fold) surfaces can be used to simulate 4- and 5-fold adsorption sites, respectively.

The 3-fold adsorption sites are most likely presented by the defects of the activated $MgCl_2$ surface. However, we assume that the local geometry of these sites can be approximated by the geometry of the relaxed $MgCl_2$ surface, which contains 3-fold Mg atoms, i.e. (1 0 0) (3-fold) surface (Fig. 3). Correctness of these assumptions will be proved in the next section, where we compare IR spectra of carbon monoxide adsorbed on three different sites of the $MgCl_2$ surface calculated within current assumptions with the corresponded experimental IR spectra.

Thus, in this section we investigate the relaxation of three $MgCl_2$ surfaces—(1 0 0) (3-fold), (1 1 0) (4-fold) and (1 0 0) (5-fold) (Figs. 1–3). In the calculations we use LDA/NCP method, since this method provides the best accuracy of the local $MgCl_2$ geometry determination (see Section 3).

4.1. (1 0 0) (3-fold) surface

A (1 0 0) (3-fold) surface contains 3-fold Mg atoms and is energetically very unfavorable. Primitive cell used in the calculations of this surface contains 4 Mg and 8 Cl atoms. This cell was translated in three directions to form so-called non-interacting $MgCl_2$ slabs. In x and y directions cell was translated in compliance with the lattice constants $a = b$ and c, whereas in z direction cell was translated to form a 10 Å wide vacuum gap between slabs (Fig. 1).

During the partial geometry optimization three bottommost atoms (1 Mg and 2 Cl atoms) were fixed in their positions in the ideal crystal.

It can be seen from Fig. 1 that optimization leads to considerable shortening of the Mg–Cl bond for the 3-fold Mg atoms.

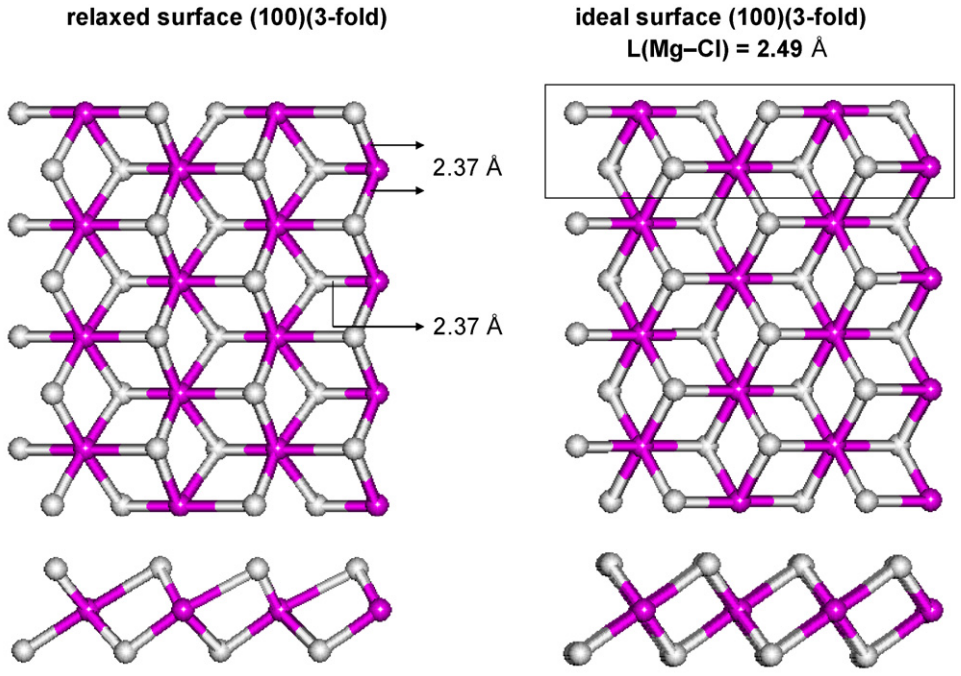

Fig. 1. Ideal and relaxed (1 0 0) (3-fold) $MgCl_2$ surfaces. Light atoms, Cl; dark atoms, Mg. Primitive cell is enclosed in rectangular frame.

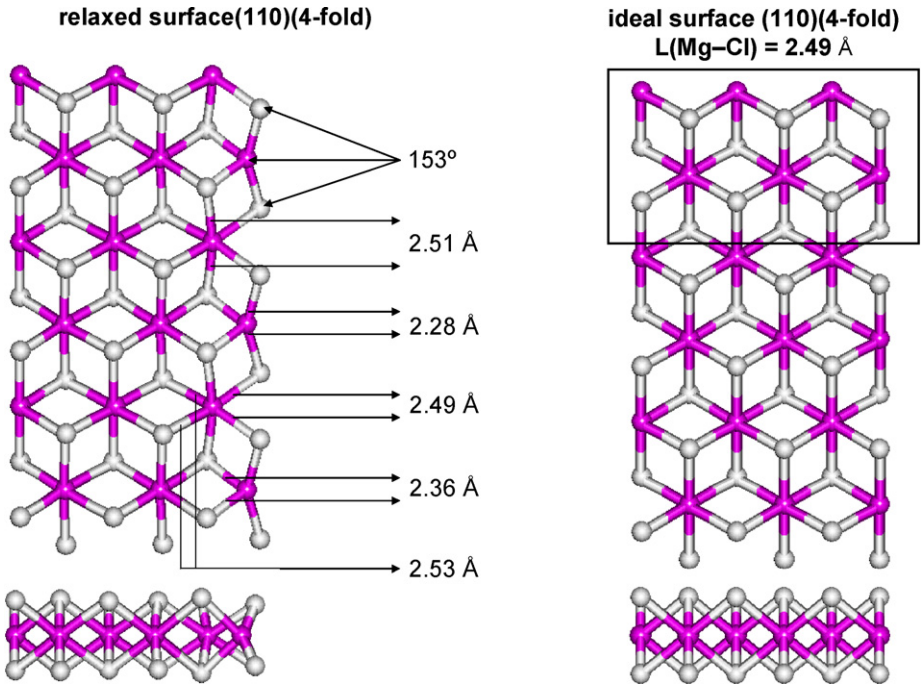

Fig. 2. Ideal and relaxed (1 1 0) (4-fold) $MgCl_2$ surfaces. Light atoms, Cl; dark atoms, Mg. Primitive cell is enclosed in rectangular frame.

Bond length decreases by approximately 5% from the ideal crystal value of 2.49–2.37 Å.

4.2. (1 1 0) (4-fold) surface

Primitive cell used in the calculations of this surface contains 6 Mg and 12 Cl atoms. During the partial geometry optimization three bottommost atoms were fixed in their positions in the ideal crystal (Fig. 2).

In contrast to the previous case $MgCl_2$ slab contains (1 1 0) (4-fold) surface on both sides. Thus, in addition to partial geometry optimization with the frozen bottom surface of the slab, full optimization of both surfaces was also performed. It was found that partial and full optimizations lead to the same geometry of the (1 1 0) (4-fold) surface. The lengths of Mg–Cl bond on the surface differ by only 0.01 Å in both cases, i.e. surface relaxation processes do not penetrate deeper than the depth of the $MgCl_2$ slab. Consequently, one could say that the size of the primitive

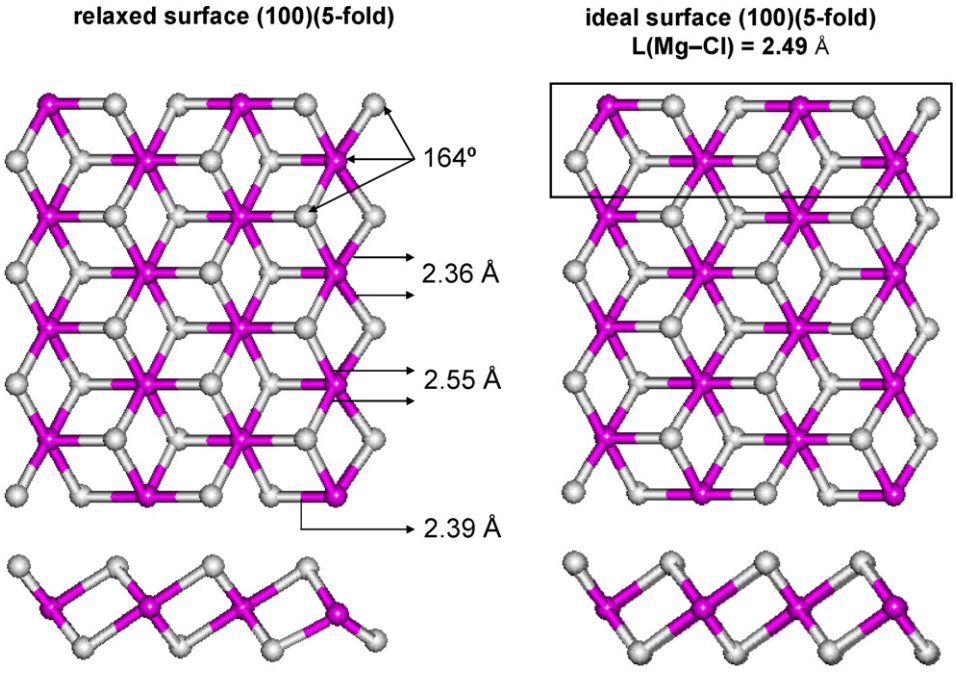

Fig. 3. Ideal and relaxed (1 0 0) (5-fold) $MgCl_2$ surfaces. Light atoms, Cl; dark atoms, Mg. Primitive cell is enclosed in rectangular frame.

cell we used is enough for adequate simulation of the $MgCl_2$ surface relaxation.

It can be seen from Fig. 2 that optimization leads again to considerable shortening of the Mg–Cl bond on the surface. Maximum observed bond length shortening was approximately 8%—from the ideal crystal value of 2.49–2.28 Å. On the whole, optimization makes Mg atoms to be slightly merged into relaxed $MgCl_2$ (1 1 0) (4-fold) surface in comparison with the ideal surface.

4.3. (1 0 0) (5-fold) surface

Primitive cell used in the calculations of this surface contains 4 Mg and 8 Cl atoms. During the partial geometry optimization three bottommost atoms were fixed in their positions in the ideal crystal (Fig. 3). In addition to partial optimization full optimization has been performed as well. It was found that partial and full optimizations lead to the same geometry of the $MgCl_2$ (1 0 0) (5-fold) surface as they do for (1 1 0) (4-fold) surface.

Optimized (1 0 0) (5-fold) surface is shown in Fig. 3. It can be seen that some Mg–Cl bonds shorten whereas some become longer, but in general Mg atoms merge into relaxed (1 0 0) (5-fold) surface.

5. The adsorption of CO

In this section we present the results of the simulation of CO binding to the $MgCl_2$ surface. The calculations, as it was already mentioned, were based on three different models of the $MgCl_2$ surface.

The first model is the Mg_6Cl_{10} frozen cluster cutout from the bulk of ideal $MgCl_2$ crystal (Fig. 4). The size and the shape of this cluster were chosen in concordance with following conditions. The cluster should contain all possible adsorption sites: 3-, 4- and 5-fold Mg atoms, i.e. the edge of the cluster should be presented with three crystallographic surfaces: (1 0 0) (3-fold), (1 1 0) (4-fold) and (1 0 0) (5-fold). Moreover, cluster should not have dangling Mg–Cl bonds and should possess the minimum possible size.

The second model is the cluster analogous to the one described above, but with unfrozen adsorption site.

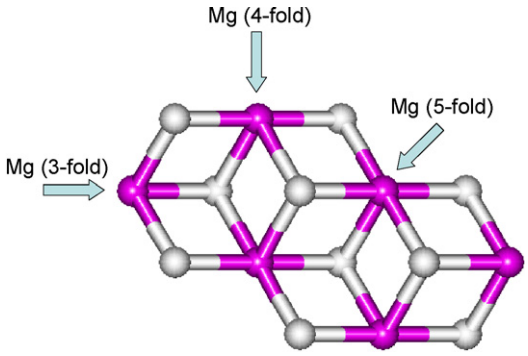

Fig. 4. Ideal Mg_6Cl_{10} cluster. The arrows point to three possible adsorption sites.

The third model is the clusters Mg_6Cl_{10} cutout from the relaxed $MgCl_2$ surfaces as it is shown in Fig. 5. The size and the shape of these clusters were kept the same for the sake of simplicity.

5.1. The adsorption of CO on ideal $MgCl_2$ clusters with totally fixed geometry

The geometries of carbon monoxide adsorbed on different sites of the ideal cluster with the frozen geometry are shown in Fig. 6. The corresponding bonds lengths L(Mg–C) and L(C=O), IR frequencies υ(C=O) and adsorption energies are summarized in Table 2 (the results obtained within frozen ideal cluster approximation are marked as *ideal fixed*). Experimental data on υ(C=O) vibration frequencies [7] is also presented in table and will be compared to the corresponding calculated values.

It can be easily seen that all calculated υ(C=O) frequencies of adsorbed CO are systematically shifted toward the UV region by approximately 30 cm^{-1} in comparison with the experimental data. Such a noticeable misfit we attribute to the neglecting of the $MgCl_2$ surface relaxation effects.

The blue shift of υ(C=O) frequencies indicates that within current ideal model of the $MgCl_2$ surface Mg atoms are stronger adsorption centers than they are in the experiment [11,23]. Obviously, relaxation processes, which were not considered in current approximation, will lead to the partial screening of magnesium atoms by chlorines and as a result to the reduction of strength of adsorption sites.

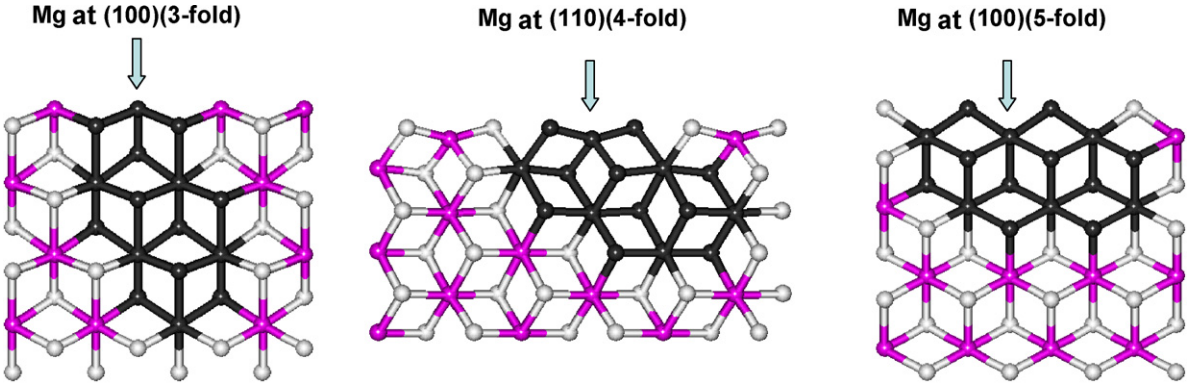

Fig. 5. Relaxed Mg_6Cl_{10}. Atoms, which compose relaxed clusters, are painted in black color.

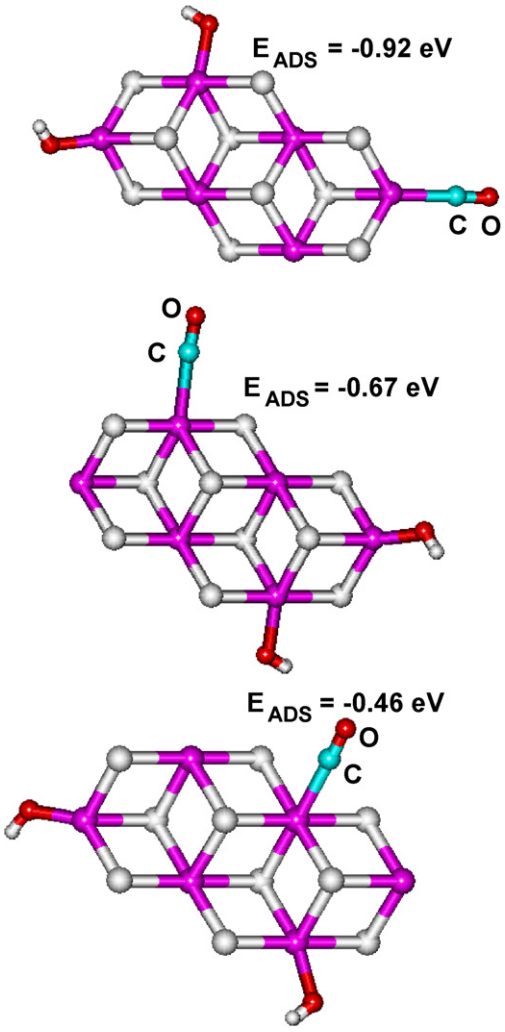

Fig. 6. Optimized geometry of the carbon monoxide bounded to different adsorption sites of the ideal Mg_6Cl_{10} cluster.

Table 2
Geometries, IR bands and adsorption energies of the CO bounded to the adsorption sites of the $MgCl_2$ surface: values obtained within different $MgCl_2$ surface models are compared with the experimental values

	ν(CO) (cm^{-1})			E_{ADS} (eV)		
	3-Fold	4-Fold	5-Fold	3-Fold	4-Fold	5-Fold
Expt.	2210	2190	2170	–	–	–
Ideal fixed	2243	2216	2194	−0.92	−0.67	−0.46
Ideal free	2235	2216	2194	−0.80	−0.67	−0.46
Relax	2213	2182	2178	−0.78	−0.28	−0.29
	L(Mg–C) (Å)			L(C=O) (Å)		
	3-Fold	4-Fold	5-Fold	3-Fold	4-Fold	5-Fold
Ideal fixed	2.32	2.35	2.41	1.126	1.129	1.131
Ideal free	2.34	2.36	2.41	1.127	1.129	1.131
Relax	2.33	2.69	2.55	1.127	1.133	1.133

5.2. The adsorption of CO on ideal $MgCl_2$ clusters with the free adsorption site

To take relaxation effects into account we allowed the adsorption site to move freely during adsorbed CO geometry optimization. The corresponded results are presented in Table 2 and are marked as *ideal free*. In comparison with the calculations with a fixed adsorption site, frequency υ(C=O) slightly changes in the case of adsorption on 3-fold Mg atom only. However, as it can be seen from Table 2 general misfit with the experiment remains unaltered.

Hence, the model with a free adsorption site is not appropriate for precise simulation of the surface relaxation effects.

Let us note that besides calculations with a free adsorption site we carried out a number of calculations with more than one free atom in the Mg_6Cl_{10} cluster. However, simultaneous unfreezing of several atoms in relatively small cluster leads to substantial distortion of the cluster geometry and does not provide compliance with the experiment.

For consecutive and more accurate simulation of the surface relaxation effects we carried out calculations using so-called relaxed clusters of magnesium chloride.

5.3. The adsorption of CO on relaxed $MgCl_2$ clusters

The geometries of carbon monoxide adsorbed on three different relaxed clusters with the frozen geometry are shown in Fig. 7. The corresponding bonds lengths L(Mg–C) and L(C=O), IR frequencies υ(C=O) and adsorption energies are summarized in Table 2 (the results obtained within frozen relaxed cluster approximation are marked as *relax*).

It can be seen that relaxed clusters approximation provides accuracy better than $10\,cm^{-1}$ of the determination of the IR spectra of the adsorbed CO.

Shift of the IR bands toward the red region implies that $MgCl_2$ adsorption sites in relaxed clusters approximation are weaker than they are in the ideal surface approach. Such weakening of the adsorption sites results from surface relaxation processes, namely from screening of Mg atoms by neighboring chlorines. Observed agreement with the experimental IR frequencies indicates that relaxed clusters, cutout from the relaxed $MgCl_2$ surface, account surface relaxation effects properly. Such an agreement allows us to conclude that the adsorption sites on the activated $MgCl_2$ surface are mainly 3-, 4- and 5-fold Mg atoms, and the structure of these sites corresponds to the structure of relaxed crystallographic $MgCl_2$ faces—(1 0 0) (3-fold), (1 1 0) (4-fold) and (1 0 0) (5-fold).

Relaxed clusters model leads to significantly lower energies of CO binding to 4- and 5-fold adsorption sites than the ideal model does. However, the energies of CO binding to 3-fold adsorption site do not differ significantly within current approximations.

The energies of CO binding to 4- and 5-fold sites are very close to each other that is in accord with the results of the work [4] where the authors could not distinguish 4- and 5-coordinated centers on the $MgCl_2$ surface by the temperature-programmed desorption (TPD) of physisorbed mesitylene.

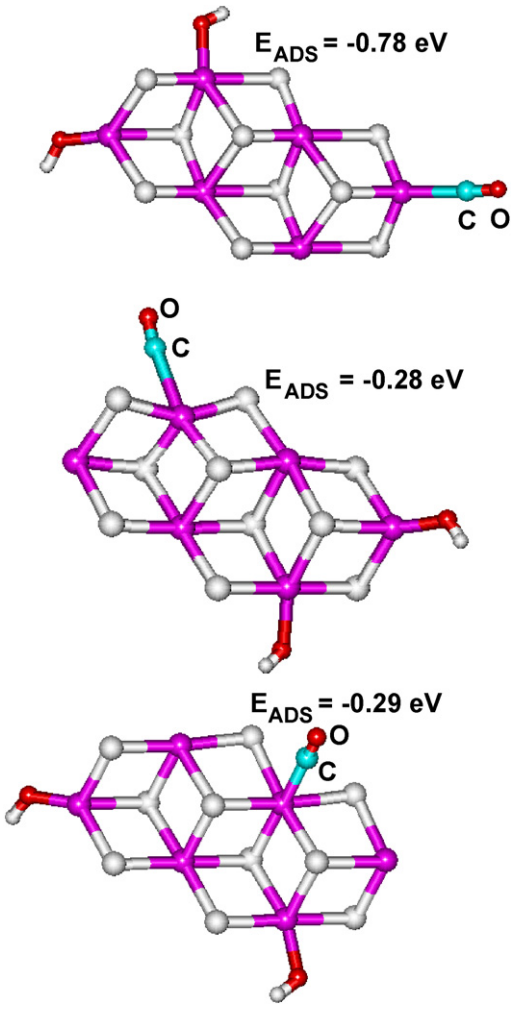

Fig. 7. Optimized geometry of the carbon monoxide bounded to different adsorption sites of the relaxed Mg_6Cl_{10} clusters.

6. Conclusions

We have optimized the geometry of the CO adsorbed on different adsorption sites of the activated $MgCl_2$ surface and calculated corresponding IR spectra of adsorbed CO using different models of the surface.

It has been found that frequencies υ(C=O) of the adsorbed CO calculated within widely used ideal cluster model are systematically shifted toward the UV region by approximately 30 cm^{-1} in comparison with the experimental data. That indicates that the adsorption sites within the ideal cluster model are much stronger than they are in the experiment.

Relaxed clusters model in combination with ab initio quantum-chemical methods described above provided agreement between experimental and calculated IR spectra within accuracy better than 10 cm^{-1}, i.e. experimental accuracy.

Such an agreement allows us to conclude that the adsorption sites on the activated $MgCl_2$ surface are mainly 3-, 4- and 5-fold Mg atoms, and the structure of these sites follows the structure of relaxed crystallographic $MgCl_2$ faces—(1 0 0) (3-fold), (1 1 0) (4-fold) and (1 0 0) (5-fold).

The very accurate determination of the IR spectra of the adsorbed CO within proposed relaxed clusters model of the $MgCl_2$ surface allows us to hope that current approach can be used for the precise simulation of different compounds binding to the $MgCl_2$ surface forming catalytic active sites of the Ziegler–Natta catalysts.

Acknowledgements

This work was supported by the Russian Foundation for Basic Research, grant 05-03-32841-a. The authors are also grateful to Sergey Malykhin for technical support.

References

[1] P.C. Barbe, G. Ceccin, L. Noristi, Adv. Polym. Sci. 81 (1987) 1.
[2] J.J.A. Dusseault, C.C. Hsu, J.M.S. Rev. Macromol. Chem. Phys. C33 (1993) 103.
[3] H. Mori, M. Sawada, T. Higuchi, K. Hasebe, N. Otsuka, M. Terano, Macromol. Rapid Commun. 20 (1999) 245.
[4] S.H. Kim, C.R. Tewell, G.A. Somorjai, Langmuir 16 (2000) 9414.
[5] V.D. Noto, R. Zannetti, M. Viviani, C. Marega, A. Marigo, S. Bresadola, Macromol. Chem. 193 (1992) 1653.
[6] D. Fregonese, A. Glisenty, S. Mortara, G.A. Rizzi, E. Tondello, S. Bresadola, J. Mol. Catal. A: Chem. 178 (2002) 115.
[7] V.A. Zakharov, E.A. Paukshtis, T.B. Mikenas, A.M. Volodin, E.N. Vitus, A.G. Potapov, Macromol. Symp. 89 (1995) 55.
[8] M. Seth, P.M. Margl, T. Ziegler, Macromolecules 35 (2002) 7815.
[9] L. Brambilla, G. Zerbi, S. Nascetti, F. Piemontesi, G. Morini, Macromol. Symp. 213 (2004) 287.
[10] G. Monaco, M. Toto, G. Guera, P. Corradini, L. Cavallo, Macromolecules 33 (2000) 8953.
[11] N.U. Zhanpeisov, E.A. Paukshtis, G.M. Zhidomirov, V.A. Zakharov, Catal. Lett. 29 (1994) 209.
[12] D.M. Ceperley, B.J. Alder, Phys. Rev. Lett. 45 (1980) 566;
J.P. Perdew, A. Zunger, Phys. Rev. B 23 (1981) 5048.
[13] J.P. Perdew, K. Burke, M. Ernzerhof, Phys. Rev. Lett. 77 (1996) 3865.
[14] J.P. Perdew, J.A. Chevary, S.H. Vosko, K.A. Jackson, M.R. Pederson, C. Fiolhais, Phys. Rev. B 46 (1992) 6671.
[15] D.R. Hamann, M. Schlüter, C. Chiang, Phys. Rev. Lett. 43 (1979) 1494;
G.B. Bachelet, D.R. Hamann, M. Schlüter, Phys. Rev. B 26 (1982) 4199.
[16] D. Vanderbilt, Phys. Rev. B 41 (1990) 7892.
[17] S. Baroni, A. Dal Corso, S. de Gironcoli, P. Giannozzi, C. Cavazzoni, G. Ballabio, S. Scandolo, G. Chiarotti, P. Focher, A. Pasquarello, K. Laasonen, A. Trave, R. Car, N. Marzari, A. Kokalj, http://www.pwscf.org/.
[18] A.D. Becke, J. Chem. Phys. A 98 (1993) 5648.
[19] M.J. Frisch, et al., Gaussian 98, Revision A.11.1, Gaussian Inc., Pittsburgh, PA, 2001.
[20] I.W. Bassi, F. Polato, M. Calcaterra, C.J. Bart, Z. Kristallogr. 159 (1982) 297.
[21] E.P. Moore Jr., Polypropylene Handbook, Hanser Publishers, New York, 1996.
[22] E. Albizzati, M. Galimberty, U. Giannini, G. Morini, Macromol. Chem., Macromol. Symp. 48–49 (1991) 223.
[23] K.M. Neyman, V.A. Nasluzov, G.M. Zhidomirov, Catal. Lett. 40 (1996) 183.